Diffusion, the Kirkendall effect and vacancy jump frequency ratios in dilute Al-Zn alloys

1994 J. Phys.: Condens. Matter 6 1985

(http://iopscience.iop.org/0953-8984/6/10/016)

J. Phys.: Condens. Matter 6 (1994) 1985–1998. Printed in the UK

Diffusion, the Kirkendall effect and vacancy jump frequency ratios in dilute Al–Zn alloys

H Hagenschulte and Th Heumann

Institut für Metallforschung, Universität Münster, Wilhelm-Klemm-Strasse 10, D-48149 Münster, Germany

Received 12 October 1993

Abstract. The method of vapour–solid couples was applied in order to investigate interdiffusion and intrinsic diffusion in dilute Al–Zn alloys. Although an aluminium oxide layer could not be avoided in our experiments, typical concentration–penetration curves were measured by electron probe microanalysis. The Boltzmann–Matano evaluation of the profiles yielded interdiffusion coefficients in agreement with previously published results.

Contrary to the expected behaviour, bulges were observed by metallographic inspection at those regions of surfaces where zinc diffused into the samples. From results of interdiffusion and from measurements with only 1 h diffusion time, it is deduced that the penetration of Zn atoms is nearly unaffected by the surface oxide layer and shows no local differences. Therefore, the reason for the growth of the bulges is the diffusion of the host component Al, which is possible only at preferred sites of the oxide layer.

The ratio D_{Zn}/D_{Al} was determined at those sites where the oxide layer was penetrated by both Zn and Al atoms. From the value measured for an infinitely dilute solution, $(D_{Zn}/D_{Al})_0 = 1.70 \pm 0.25$, the vacancy flow factor $(L_{AlZn}/L_{ZnZn})_0 = -0.19 \pm 0.13$ was derived. Vacancy jump frequency ratios according to the five-frequency model were calculated, which differ from unity only slightly and are similar to those obtained for the systems Ag–Zn and Cu–Zn. A weak binding between vacancies and Zn impurity atoms was estimated by means of two different methods.

1. Introduction

A detailed picture of the diffusion behaviour of infinitely dilute binary substitutional alloys with FCC structure is given by the so-called five-frequency model [1–3]. Assuming that only monovacancies interact with isolated impurity atoms, the three vacancy jump frequency ratios w_4/w_0, w_2/w_1 and w_3/w_1, with w_i defined in the usual way, are related to the following four experimentally obtainable quantities: the ratio of solute and solvent tracer diffusion coefficients $(D_B^*/D_A^*)_0$, the correlation factor f_B of impurity diffusion, the linear enhancement factor b_1 of solvent diffusion and the vacancy flow factor $(L_{AB}/L_{BB})_0$. The infinitely dilute state is indicated by the index 0. Experimental results for at least of three of these quantities are required for the determination of jump frequency ratios.

For aluminium systems our knowledge of vacancy jump frequency ratios is confined to a few estimations [4] and one set of data for the system Al–Fe obtained by Mößbauer spectroscopy [5]. Two experimental difficulties in diffusion measurements with aluminium and its alloys are the main reason for these limitations: for the measurement of solvent diffusion with the reliable radiotracer method only the isotope ^{26}Al is available; this isotope, however, is unsuitable for diffusion experiments because of its very long half-life and its very low specific activity. This is why experimental results for the enhancement factor b_1

0953-8984/94/101985+14$19.50

are unknown for Al systems. Therefore, for the determination of jump frequency ratios the vacancy flow factor $(L_{AB}/L_{BB})_0$ is required. This is related to the ratio of the intrinsic diffusion coefficients $(D_B/D_A)_0$ according to [6]

$$\left(\frac{L_{AB}}{L_{BB}}\right)_0 = \left(\frac{D_A^*}{D_B^*}\right)_0 \frac{1}{f_0} - \left(\frac{D_A}{D_B}\right)_0 \frac{\bar{V}_B}{\bar{V}_A} \tag{1}$$

where $\bar{V}_{A,B}$ is the partial molar volume of component A, B and $f_0 = 0.7815$ is the correlation factor of pure FCC metal A.

The ratio of individual diffusion coefficients D_B/D_A is obtained from the motion of inert markers in Kirkendall-effect experiments. For this purpose the shift of welding interfaces is usually measured, for example by means of the so-called thin-plate method [7]. The welding of couples with different compositions is required for this kind of measurement. Aluminium and aluminium alloys, however, are always coated by a naturally grown surface oxide layer, which may considerably affect the welding and the following diffusion process. Reliable results cannot be expected in this case.

For this reason, the method of vapour–solid couples, which was first applied by Balluffi and co-workers [8,9], was chosen to investigate intrinsic diffusion in an Al system. This allows the determination of the ratio D_B/D_A, with the practical advantage that no welding of diffusion couples is required. In this type of diffusion couple a high-vapour-pressure component B diffuses into a slab of pure metal A with negligible vapour pressure at the annealing temperature.

The element Zn was chosen as the solute component since it satisfies the thermodynamic requirements of a high vapour pressure [10] and a sufficient solubility [11]. For the system Al–Zn, data from tracer diffusion coefficients, D_{Zn}^*, D_{Al}^*, and correlation factors, f_{Zn}, are additionally available [12], so that all the quantities required for an evaluation of jump frequency ratios are either measurable or known.

2. Method of vapour–solid couples

2.1. Principle and expected behaviour in the case of undisturbed diffusion

A slab of pure Al with inert markers on its surface is exposed to Zn vapour. During the diffusion time the initial sample length at $t = 0$, d_0, increases due to absorption of Zn atoms from the vapour phase. Figure 1 shows schematically the situation before and after the diffusion anneal of such a vapour–solid couple. Because of the mirror symmetry of the two end faces of the specimen, only the left face is shown in figure 1. At this face Zn atoms diffuse into the slab from left to right. Due to the process of interdiffusion a flux of Al atoms in the opposite direction also occurs. Diffusion of the two components leads to a concentration–penetration curve, as shown in figure 1.

In the following, constant solute concentration at the vapour–solid interface and constant partial molar volumes $\bar{V}_i$ are assumed. If the penetration depth during the annealing time is much smaller than the sample length, i.e. $\sqrt{\tilde{D}t} \ll d_0$, the condition of a semi-infinite couple is fulfilled and interdiffusion coefficients can be determined by applying the usual Boltzmann–Matano analysis [9, 13]. In the case considered, the position of the Matano interface remains identical with the position of the initial surface during the entire diffusion process.

The difference of Al and Zn diffusion fluxes gives rise to a Kirkendall shift of the marker interface, which is initially also identical with the original surface. As a rule, the

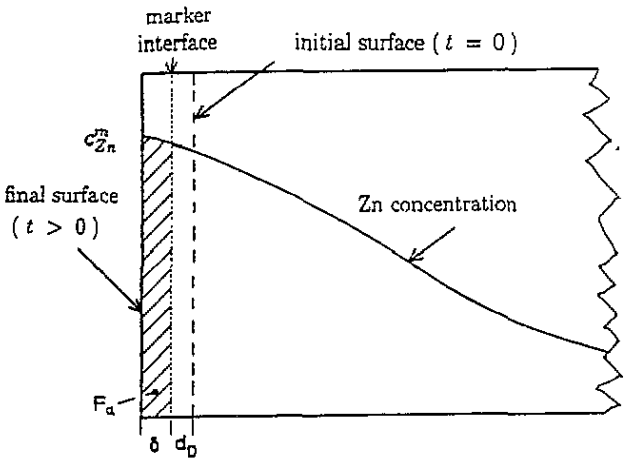

Figure 1. Method of vapour–solid couples, schematically.

component with the higher vapour pressure also has a higher mobility [9]. Therefore, the marker interface, which is shifted in the opposite direction to the mass flow of the faster diffusing component Zn, is found at a distance δ, which is smaller than the increase in sample length given by $d_D + \delta$. The ratio of the intrinsic diffusion coefficients D_{Zn}/D_{Al} may be determined by the following equation:

$$\frac{D_{Zn}}{D_{Al}} = \frac{(d_D + \delta) - \bar{V}_{Zn} F_a}{\delta - \bar{V}_{Zn} F_a}. \tag{2}$$

Here F_a is the small hatched area shown in figure 1, and is approximately given by the product $F_a \approx c^m_{Zn}\delta$, where c^m_{Zn} denotes the Zn concentration at the marker interface. For the derivation of (2) we refer to [14].

The increase in sample length $d_D + \delta$ is closely linked to the amount of Zn absorbed from the vapour. It can be calculated either from the increase in sample weight, by taking the geometry of the slab into account, or by an integration of the concentration–penetration curve. Using an optical microscope the distance δ is easily obtained, if the marker interface can be made visible by a suitable etching technique. Uncertainty in the measurement of δ is the main source of error for the ratio D_B/D_A. For this reason the method of vapour–solid couples is particularly suitable for systems with $D_B/D_A \approx 1$. In this case the precision of the measurement of δ increases because comparably large values of δ are obtained.

2.2. *Experimental procedure*

Aluminium single crystals of 8 mm diameter were grown from 99.999% pure Al in an Ar atmosphere in graphite crucibles by the Bridgman method. After a pre-anneal in evacuated quartz capsules for one week at 870 K the rods were cut into cylindrical specimens of 6 mm thickness by means of spark erosion. The end faces of each sample were ground on waterproof abrasive papers and polished in three stages on metallographic cloth with 15 μm, 6 μm and 1 μm diamond agent.

Alloys containing a few at.% Zn were melted from appropriate amounts of pure Al and Zn by RF heating. In order to achieve a better mixing of the two components the alloys were melted for a second time and homogenized for three days at 870 K in quartz capsules filled with Ar gas. The homogeneity was finally checked using electron probe microanalysis

(EPMA). Finally, the alloy rods were machined on a lathe into chips, so increasing the surface-to-volume ratio and easing the conversion of Zn atoms into the vapour phase.

Together with an aluminium sample, for which preparation was finished just in time, the alloy chips were subsequently sealed in a large quartz ampoule ($\varnothing \approx 25$ mm, $l \approx 30$ cm). This ampoule was evacuated to a pressure lower than 10^{-6} hPa. Constancy of the Zn equilibrium vapour pressure during the annealing time was ensured by the large amount of alloy chips, which was at least 30 times as large as the sample weight.

Our first attempts showed that the conversion of Zn atoms into the vapour phase was considerably reduced for alloy chips that had been in contact with oxygen in the air for several days. A drastic reduction of this conversion was also observed if the ampoule had been opened after an anneal for a change of the sample for another experiment with the same alloy chips. In this case the diffusion of Zn out of the chips was nearly stopped, even by a short contact with air. For these reasons, only newly machined alloy chips were used for final reported experiments.

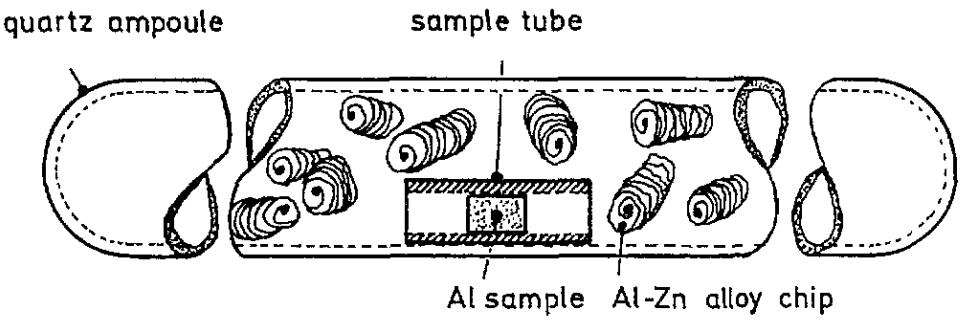

Figure 2. Arrangement of Al–Zn alloy chips and of an Al specimen in the quartz ampoule.

As shown in figure 2, the Al sample was arranged in a special tube of graphite or quartz in order to avoid direct contact between the chips and the sample. The diameter of the tube was tight enough to ensure a good contact at the annealing temperature of the cylinder surface of the sample with the wall of the tube. Therefore, Zn atoms could diffuse only via the end faces into the slab, thus allowing a simple calculation of the increase in sample length from its increase in weight.

The annealing treatments at a temperature $T = 829$ K were carried out in an electric resistance furnace controlled within ± 1 K. The furnace was long enough to provide an equal-temperature region exceeding the length of the quartz ampoules. From data on the thermodynamic activity of dilute Al–Zn alloys [10] a Zn equilibrium vapour pressure between 0.7 and 3.2 hPa is to be expected, depending on the Zn concentration of the alloy chips, which was chosen between 2 and 9.2 at.%.

3. Results

3.1. Concentration–penetration curves and interdiffusion coefficients

After the diffusion anneal the samples were weighed again and cut parallel to the diffusion direction. Subsequently, the sectional planes were polished as described above and

concentration–penetration curves were taken by means of electron probe microanalysis. In figure 3 we show two penetration profiles taken from opposite end faces of a sample that was annealed for 115.3 h at $T = 829$ K with alloy chips containing 4.5 at.% Zn. Despite the surface oxide layer a large amount of Zn diffused into the sample. In the present case the maximum value of the penetration depth exceeds 1500 μm. The penetration curves are typical for the method of vapour–solid couples and show no irregularities. This may also be checked by a determination of the Zn concentration at the surface, which is only slightly lower than the Zn concentration of the alloy chips.

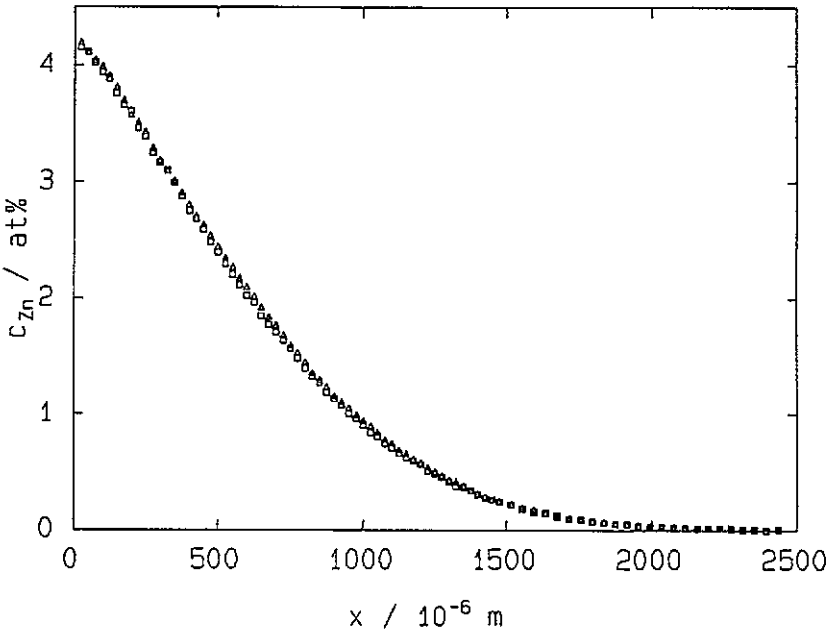

Figure 3. Concentration–penetration curves; $t = 115.3$ h; $T = 829$ K; concentration of alloy chips: 4.5 at.% Zn; △ profile taken at the left-end face; □ profile taken at the right-end face.

Using the constant partial molar volumes $\bar{V}_{Zn} = 10.00 \times 10^{-6}\,m^3\,mol^{-1}$ and $\bar{V}_{Al} = 9.42 \times 10^{-6}\,m^3\,mol^{-1}$ [15] interdiffusion coefficients were calculated by applying the usual Boltzmann–Matano method. The results for some experiments with different Zn concentrations of alloy chips are given in figure 4. The interdiffusion coefficients of the measurement with 9.2 at.% Zn represent mean values for all evaluated experiments. The deviations of the two other curves from the 9.2 at.% curve indicate the scattering of the measurements.

Our results are in qualitative agreement with interdiffusion measurements carried out at lower temperatures by Hilliard and co-workers [16]. The mean value $\tilde{D}(0) = 5.95 \times 10^{-13}\,m^2\,s^{-1}$ was obtained by extrapolation to an infinitely dilute solution. Taking possible temperature differences into account the agreement of this value with comparable Zn tracer diffusion coefficients $D^*_{Zn}(0)$, which are also shown in figure 4, is quite reasonable given the limitations of the vapour–solid couple technique. From these results it can be concluded that the influence of the surface oxide layer on Zn diffusion into the Al samples is weak.

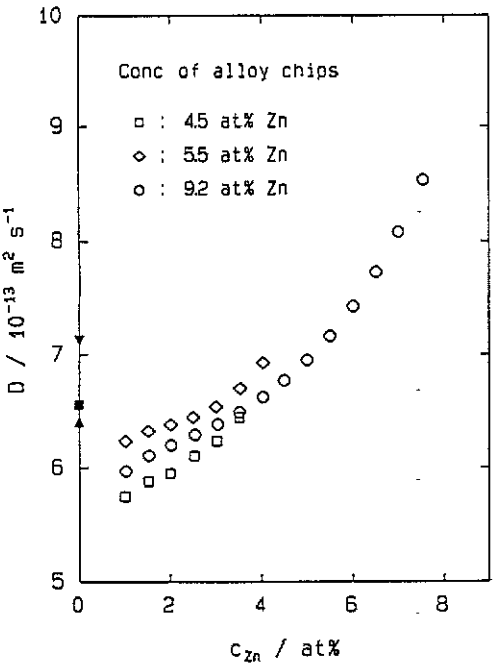

Figure 4. Concentration dependence of interdiffusion coefficients in dilute Al–Zn alloys and tracer diffusion coefficients from the literature: ▼ [17], ■ [18], ▲ [19].

3.2. Observation of bulges at the surface

The photomicrographs of figure 5(*a*), (*b*) show details of a sample that was cut perpendicular to the end faces. In both pictures, Zn diffused from left to right into the originally pure Al so the situation corresponds to the schematic picture of figure 1. In contrast to that diagram the surface topography is clearly different. Bulges, which often have a longish oval shape, can be observed at the surface. A superficial inspection indicated that many bulges of a single sample were uniform in height, but a distribution in the height of the bulges was observed.

The number and size of grown bulges varied appreciably, even under the same experimental conditions. In some cases only a few single bulges could be observed, while in others the surface was nearly covered. Nevertheless, a tendency toward greater growth rates of the bulges was linked to increasing Zn concentrations in the alloy chips.

In particular, it is noteworthy that a marker line appeared at the bottom of every bulge. This marker line may already be recognized in figure 5. In figure 6 two micrographs of another sample are shown; the marker line became clearly visible by utilizing the following etching procedure: 3 ml HF + 100 ml H_2O; 1–2 s; short dip in pure H_2O; 20 mg NaOH + 40 ml H_2O; 1–2 min. The coincidence of the marker line with the line of the remaining surface is clearly to be seen in figure 6(*a*). Figure 6(*b*) shows a cut at a site where the surface was completely covered.

3.3. Interpretation of bulge growth

3.3.1. Diffusion behaviour of Al and Zn atoms. For the interpretation of bulge growth it should be kept in mind that the Al specimens used were always coated by a naturally grown surface oxide layer of unknown thickness. Since the bulges have not been observed in systems having no oxide layers, for example in Ag–Zn and Ag–Cd systems [20, 21], the

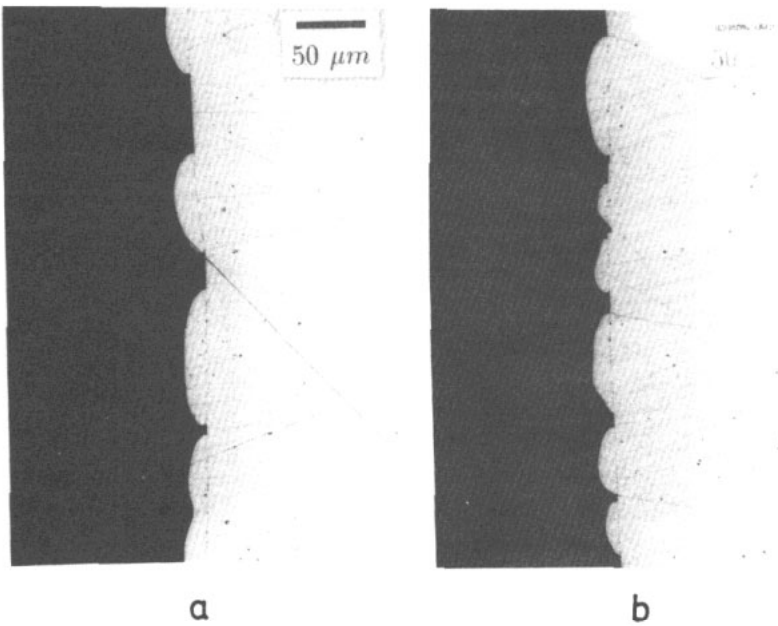

Figure 5. Optical micrographs of an Al sample into which Zn has diffused; concentration of alloy chips: 5.5 at.% Zn; $T = 829$ K; $t = 111.75$ h.

growth of the bulges may be explained by interference of the normal diffusion behaviour of the two components from the oxide layer.

At first glance it seems to be possible to assume that local differences in the diffusion rates of the solute component Zn between sites with bulges and those without bulges could give rise to their occurrence. To verify this assumption, the Zn concentration was measured near the surface by EPMA. The two lines along which measurements have been made are depicted schematically in figure 7(*a*). The resulting penetration curves of the first 60 μm for a site with a bulge and for a site without a bulge are shown in figure 7(*b*). For both readings the zero point of the x axis is defined to coincide with the vapour–solid interface.

Volatilization of Zn during the cooling to room temperature is the reason for reduced Zn concentrations in the first 15 μm. Obviously the two penetration curves are almost identical. This finding alone, however, does not permit the conclusion that there are no differences between Zn diffusion at sites with a bulge and those without a bulge. Because of the great penetration depth, corresponding to an annealing time of 115.3 h, the concentration distribution of figure 7(*b*) would also be obtained if Zn atoms diffused preferentially into the slab at sites with a bulge and a lateral mass flow equalized the concentration gradients along lines perpendicular to the surface. This conceivable behaviour is illustrated by the arrows in figure 7(*a*).

In order to obtain a clearer picture experiments under the same conditions, but with an annealing time of only one hour, were carried out. For this short annealing period, a levelling of concentrations by lateral mass flow can be excluded. Therefore, Zn concentration gradients should have been observed near the surface along the direction of the vertical arrows in figure 7(*a*). The local Zn concentrations of samples with an annealing time of one hour were measured at a depth of 10 μm parallel to the surface by EPMA with the result that no concentration gradients in the lateral diffusion direction were observed. This finding

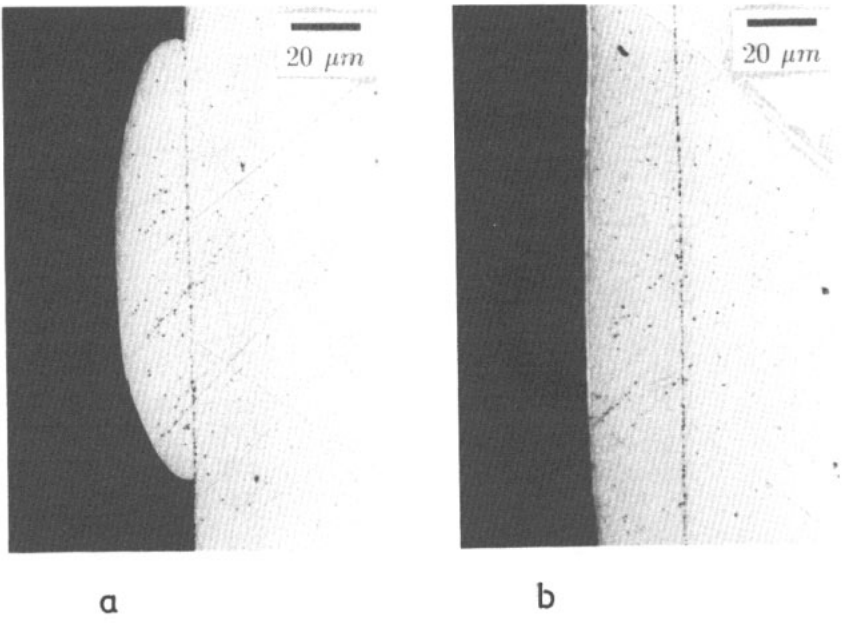

Figure 6. Optical micrographs showing the marker line (*a*) at a single bulge and (*b*) at a region where the surface was completely covered. Experimental conditions as follows. Concentration of alloy chips: 5.45 at.% Zn; $T = 829$ K; $t = 310.5$ h.

shows that there are no preferred sites for the diffusion of Zn through the aluminium oxide layer.

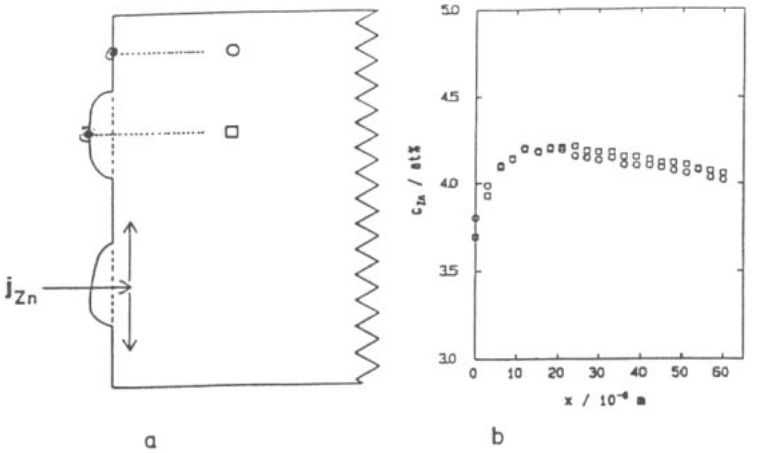

Figure 7. (*a*) Schematic drawings of bulges; arrows indicate a possible preferred diffusion of Zn at a site of a bulge and a following lateral mass flow; along the dotted horizontal lines the penetration curves of (*b*) were measured. (*b*) □, site with bulge; ○, site without bulge; concentration of alloy chips: 4.5 at.% Zn; $T = 829$ K; $t = 115.3$ h.

The only difference found in experiments with shorter annealing times was a greater gap, of about 1.5 at.% Zn, between the surface concentration and the concentration of the alloy chips after an annealing time of one hour. A possible reason is that the equilibrium Zn vapour pressure is not reached in the early stages of the experiment. From the interdiffusion coefficients it is evident that this initial disturbance decreases quickly with diffusion time.

To summarize, the diffusion behaviour of the Zn component can be described as follows. With the exception of a small disturbance at the beginning of the annealing process, the diffusion of Zn atoms is nearly unaffected by the oxide layer. The Zn atoms adsorbed from the vapour phase penetrate the aluminium oxide layer everywhere in the same way, so the diffusion of the solute component Zn cannot explain the occurrence of the bulges.

We must therefore conclude that the diffusion behaviour of the solvent component Al through its own oxide layer gives rise to the growth of the bulges. In the case shown in figure 7(*b*), more than 95 at.% of the contents of the bulges is Al. This Al has diffused past the marker line, which apparently coincides with the oxide layer. At the sites where bulges grow, the Al diffuses through its own oxide layer just as the Zn diffuses in the opposite direction. This is the behaviour expected at vapour–solid couples for samples without an oxide layer.

This interpretation explains the occurrence of the marker line, its coincidence with the remaining surface and the uniform height of many bulges from a single sample. The uniform maximum height of the bulges corresponds to the quantity δ in figure 1. Some lower bulges are caused by partly disturbed Al diffusion. In contrast to this finding, the Al diffusion is apparently blocked by the oxide layer at those sites where no bulges grow. In those areas the values of the quantities δ and F_a are equal to 0, and equation (2) cannot be applied.

3.3.2. Possible reasons for local differences in Al diffusion. At this point the following question arises: why does Al diffusion pass through its oxide layer at those sites where bulges are grown, while it is obviously blocked everywhere else? The reason for this strange behaviour is still unclear. Preliminarily, the following possibilities are suggested.

(i) Fine cracks in the surface oxide layer may occur due to the different thermal expansion coefficients of aluminium and the oxide layer.

(ii) Bulk defects like dislocations, grain boundaries and subgrain boundaries ending at the oxide layer give rise to local differences in the structure of the layer.

(iii) Intrinsic defects exist in the structure of the surface oxide layer.

Metallographic inspection of sample surfaces subject to a one hour diffusion anneal revealed that bulge growth starts at many single and isolated points. Hundreds of these points were often arranged in groups or lines in some regions of the surface, while in other regions none could be observed. As a consequence, a great variety in the distribution of the bulges was found for experiments with longer annealing times. Isolated bulges were observed as well as closed configurations looking like grain boundary networks.

Since the heating procedure was the same for all samples, a comparable bulge distribution should be expected, if suggestion (i) was the reason for the locally different diffusion behaviour of Al. But the observed variety in bulge distribution and the growth of bulges at many single points disagrees with suggestion (i).

Although some observations indicate that the growth of the bulges is related to dislocations ending at the surface, there are also good arguments that contradict suggestion (ii). The surface dislocation density of the pre-annealed pure Al samples was, in all cases, higher by orders of magnitude than the observed bulge density. Moreover, the distribution

of dislocations is more or less regular because of repulsive interactions between the strain–stress fields. The observed configurations in groups and lines are incompatible with this regular distribution.

At present it seems most likely that intrinsic defects in the surface oxide layer give rise to locally different diffusion behaviour of Al. The existence of such defects is well known from corrosion experiments [22]. In the present case the great variety in the bulge distribution can be explained if the number of intrinsic defects strongly depends upon surface preparation. Information on the local structure and composition, which can be provided by suitable surface science methods, may clarify the question of why the diffusion of Al proceeds only at some preferred sites on the surface oxide layer.

3.4. Intrinsic diffusion coefficients

For the determination of the ratio of intrinsic diffusion coefficients according to (2) the maximum height of the bulges, which equals the quantity δ, was measured for a number of samples annealed together with alloy chips of different concentrations in the range 2–9.2 at.% Zn. The results are summarized in table 1.

Table 1. Experimental parameters and results obtained by means of the method of vapour–solid couples for the system Al–Zn.

Zn conc. of alloy chips	c^{m}_{Zn} (at.%)	Annealing time (h)	$d_D + \delta$ (μm)	δ (μm)	D_{Zn}/D_{Al}
9.20	8.90	111.25	55.0	22.5	2.58 ±0.22
7.10	6.65	87.50	39.9	18.5	2.24 ±0.23
5.45	5.20	310.50	57.7	26.5	2.24 ±0.17
5.55	5.10	101.50	28.2	14.0	2.07 ±0.29
4.50	4.25	115.30	25.8	13.5	1.95 ±0.28
3.55	3.40	111.25	19.2	9.5	2.04 ±0.38
2.30	2.15	593.50	27.2	14.0	1.96 ±0.26

The increase in sample length, $d_D + \delta$, which is caused by the amount of Zn absorbed from the vapour, was determined both by integration of the penetration curves and by measurements of the increase in sample weight. The values obtained by the two methods agree within the limits of error. For the determination of $d_D + \delta$ from the mass gain, the geometric size of the slab has to be known, so the accuracy of the values determined by integration of the penetration curves is slightly better. These values are given in table 1.

The maximum height of the bulges δ was measured with an optical microscope in bright-field illumination at a magnification of 500. Weighted average values of these heights, which were nearly uniform, are listed in table 1. In figure 6(*b*) a site is shown that apparently corresponds to the case of undisturbed diffusion behaviour at vapour–solid couples. Measurements taken at such sites have been weighted higher than those at single bulges. The mean values are accurate to within $\pm 1.5\,\mu$m.

The ratio of intrinsic diffusion coefficients was calculated applying (2). In figure 8 a nearly linear increase of the ratio D_{Zn}/D_{Al} with the solute concentration is shown up to 9 at.% Zn. In an infinitely dilute solution, the value $(D_{Zn}/D_{Al})_0 = 1.70 \pm 0.25$ is obtained by extrapolating the fitted straight line to $c_{Zn} = 0$.

Experimental results for the ratio of intrinsic diffusion coefficients at infinitely dilute solution published elsewhere are summarized in table 2 for some noble metal systems. The given temperatures are related to the corresponding melting points of the host metals. With

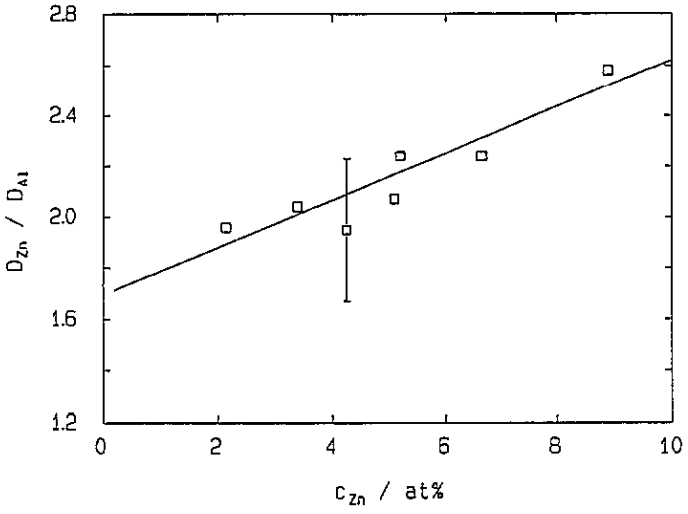

Figure 8. Ratio of intrinsic diffusion coefficients D_{Zn}/D_{Al} as a function of the Zn concentration c_{Zn}.

Table 2. Ratio of intrinsic diffusion coefficients D_B/D_A at infinitely dilute solution for some noble metal systems and for Al–Zn.

System	T/T_M	D_B/D_A	Ref.
Al–Zn	0.89	1.7	This work
Cu–Zn	0.86	2.0	[23]
Cu–In	0.74	2.20	[24]
Cu–Sn	0.80	1.95	[25]
Cu–Sb	0.74	1.54	[26]
Ag–Zn	0.83	1.04	[27]
Ag–Cd	0.87	1.38	[28]
Ag–Sb	0.85	1.51	[29]
Au–In	0.84	1.64	[30]
Au–Sn	0.85	1.56	[30]

very few exceptions the values obtained fulfill the relation $1 < (D_B/D_A)_0 < 2$. Since the value for the Al–Zn system is also in this range, our result is in accord with those for other FCC metal systems.

3.5. Jump frequency ratios and Gibbs free energy of binding

According to (1) the ratio of tracer diffusion coefficients must also be known to permit a calculation of the vacancy flow factor $(L_{AB}/L_{BB})_0$. For this purpose a mean value for $(D^*_{Zn}/D^*_{Al})_0$ was calculated from the most reliable Zn tracer diffusion measurements [17–19, 31, 32], from Al tracer diffusion coefficients [33, 34], and from an NMR measurement [35]. For $T = 829\,K$ the value $(D^*_{Zn}/D^*_{Al})_0 = 3.5 \pm 0.5$ was obtained, and by using (1) the vacancy flow factor was found to be $(L_{AlZn}/L_{ZnZn})_0 = -0.19 \pm 0.13$.

Since values of the enhancement factor of solvent diffusion, b_1, are not available, the determination of vacancy jump frequency ratios relies upon knowledge of the correlation factor of impurity diffusion, f_{Zn}. From isotope effect measurements of Zn diffusion in Al [18], the correlation factor $f_{Zn} = 0.50 \pm 0.05$ was obtained at $T = 829\,K$. An energy factor $\Delta K = 0.95$ [18] was assumed for the calculation of f_{Zn}.

The jump frequency ratios w_4/w_0, w_2/w_1 and w_3/w_1 were calculated and the results are summarized in table 3. The deviations from unity are small for all three jump frequency ratios. A comparison with values determined for noble metal systems, which have been intensively studied by many groups in the past [14], shows that the values obtained for the Al–Zn system are similar to those corresponding to the systems Ag–Zn and Cu–Zn. The jump frequency ratios obtained for these systems are also given in table 3.

Table 3. Jump frequency ratios and enhancement factor of solvent diffusion calculated for the Al–Zn system and corresponding results for Cu–Zn and Ag–Zn from literature. b_1 values from [36]; w_i/w_j from [14].

System	T (K)	T/T_M	b_1	w_4/w_0	w_2/w_1	w_3/w_1
Al–Zn	829	0.89	9.5	1.39	2.54	0.64
Cu–Zn	1168	0.86	7.7	1.24	2.68	0.56
Ag–Zn	1020	0.83	11.3	1.25	1.90	0.35

The enhancement factor of solvent diffusion, b_1, can be calculated from known jump frequency ratios. According to Howard and Manning [3] the enhancement factor b_1 is related to the jump frequency ratios as follows:

$$b_1 = -18 + \frac{4}{f_0}\frac{w_4}{w_0}\left(\chi_1\frac{w_1}{w_3} + 3.5\chi_2\right) \tag{3}$$

where χ_1 and χ_2 are average correlation factors listed in [3] for many sets of w_4/w_0, w_2/w_1 and w_3/w_1 values. Employing (3), the enhancement factor in dilute Al–Zn alloys at $T = 829\,\mathrm{K}$ was calculated to be $b_1 = 9.5 \pm 4.5$, which is similar to results obtained for Ag–Zn and Cu–Zn systems (see table 3).

The Gibbs free energy of binding, δg, of a vacancy–impurity pair was estimated by two different methods based on the well known relation between δg and the jump frequencies w_3 and w_4:

$$\frac{w_4}{w_3} = \exp\left(-\frac{\delta g}{kT}\right). \tag{4}$$

For the determination of the ratio w_4/w_3 the following equation was recently derived [37]:

$$\frac{w_4}{w_3} = 1 + \frac{[(b_1 - b_B)(b_1 - 3) + 5 + 2K](1/f_0)}{12\{(b_1 - b_B - 3)(1/f_0) + (D_B^*/D_A^*)[2K + (f_V^B/f_B) - 1]\}} + \frac{(b_1 - 1)(D_B^*/D_A^*)[2K + (f_V^B/f_B) - 1] - 2(D_B^*/D_A^*)K^2}{12\{(b_1 - b_B - 3)(1/f_0) + (D_B^*/D_A^*)[2K + (f_V^B/f_B) - 1]\}}. \tag{5}$$

Here $K = (D_A/D_B)(\overline{V}_B/\overline{V}_A)$, b_B is an enhancement factor defined by Bocquet [38] and f_V^B is the correlation factor of the vacancy when the vacancy has exchanged its place with an impurity atom. All quantities in (5) may be calculated from known jump frequency ratios.

Since its derivation does not exceed the limits of the five-frequency model, equation (5) holds strictly for the case of an infinitely dilute solution. Using the values of table 3, and combining (4) and (5), the Gibbs free energy of binding $\delta g = -0.09_8\,\mathrm{eV}$ was obtained. According to its definition a negative value of δg characterizes an attractive interaction between a vacancy and a Zn impurity atom. Since for small b_1 values the result of (5) is

sensitively related to the difference $b_1 - b_B$ [37], the estimated value should be understood as an upper limit for the attractive interaction.

Another method of estimation for δg by Arnhold and co-workers [39] suggests that the mean jump frequency of a vacancy in a vacancy–impurity complex is approximately the same as that in the pure host metal, i.e. $12w_0 \approx 4w_1 + 7w_3 + w_2$. Using this assumption, the ratio w_4/w_3 can easily be calculated from known jump frequency ratios. According to (4) this evaluation yields a Gibbs free energy of binding of $\delta g = -0.05_1$ eV.

Table 4. Enthalpy of binding δh for the Al–Zn system as obtained by means of various experimental and theoretical methods.

	δh (eV)	Method	Ref.
Exp.	−0.03	Zn tracer diffusion	[17]
	−0.02	Positron annihilation	[40]
	−0.02	Quenching	[41]
	−0.02	Quenching	[42]
Theor. calc.	−0.03	Pseudopotential	[43]
	−0.02	Oscillating potential	[43]
	−0.02	KKR–Green function	[44]

Vacancy–impurity interactions have been investigated in many theoretical and experimental works. Some results of the binding enthalpy, δh, which is related to the Gibbs free energy of binding by the well known equation

$$\delta g = \delta h - T\delta s \tag{6}$$

are summarized for the system Al–Zn in table 4; δs denotes the binding entropy. The cited values agree with our finding that the interaction between single vacancies and Zn impurity atoms is attractive and that the binding is very weak.

Acknowledgments

We are grateful to Professor V Ruth, Department of Metallurgy, University of Oldenburg, for having presented the first results of this work at the TMS Fall Meeting, October 22–25 1991, Cincinnati, OH, and for a critical reading of the manuscript. The financial support of the Deutsche Forschungsgemeinschaft is gratefully acknowledged.

References

[1] Howard R E and Lidiard A B 1964 *Rep. Prog. Phys.* **27** 161
[2] Manning J R 1965 *Phys. Rev.* **139** A2027
[3] Howard R E and Manning J R 1967 *Phys. Rev.* **154** 561
[4] Fujikawa S and Hirano K I 1987 *Mater. Sci. Forum* **13–14** 539
[5] Mantl S, Petry W, Schroeder K and Vogl G 1984 *Phys. Rev.* B **27** 5313
[6] Heumann Th 1979 *J. Phys. F: Met. Phys.* **9** 1997
[7] Heumann Th 1977 *Z. Naturf.* a **32** 54
[8] Ballufi R W and Alexander B H 1952 *J. Appl. Phys.* **23** 1237
[9] Ballufi R W and Seigle L L 1954 *J. Appl. Phys.* **25** 607

[10] Hultgren R, Desai P D, Hawkins D T, Gleiser M, Kelley K K and Wagman D D 1973 *Selected Values of the Thermodynamic Properties of Binary Alloys* (Metals Park, OH) pp 228, 571
[11] Massalski T B (ed) 1986 *Binary Alloys Phase Diagrams* (Metals Park, OH)
[12] Mehrer H (ed) 1991 *Landolt–Börnstein New Series 26: Diffusion in Metallen* (Berlin: Springer)
[13] Onishi M and Shimozaki T 1985 *Trans. Japan. Inst. Met.* **26** 799
[14] Heumann Th 1992 *Werkstoff-Forschung und Technik 10: Diffusion in Metallen* ed B Ilschner (Berlin: Springer) pp 137, 177
[15] Pearson W B 1958 *Handbook of Lattice Spacings and Structures of Metals* vol 1 (Oxford: Pergamon)
Pearson W B 1967 *Handbook of Lattice Spacings and Structures of Metals* vol 2 (Oxford: Pergamon)
[16] Hilliard J E, Averbach B L and Cohen M 1959 *Acta Metall.* **7** 86
[17] Beke D L, Gödeny I and Kedves F J 1983 *Phil. Mag.* **47** 281
[18] Peterson N L and Rothman S J 1978 *Phys. Rev.* B **17** 4666
[19] Fujikawa S and Hirano K I 1976 *Trans. Japan. Inst. Met.* **17** 809
[20] Shimozaki T, Onishi M and Ito K 1985 *Trans. Japan. Inst. Met.* **26** 385
[21] Hummert K 1994 *PhD Thesis* Universität Münster, in preparation
[22] Altenpohl D 1965 *Aluminium und Aluminiumlegierungen* (Berlin: Springer)
[23] Hoshino K, Iijima Y and Hirano K I 1982 *Met. Trans.* A **13** 1135
[24] Hoshino K, Iijima Y and Hirano K I 1981 *Phil. Mag.* **44** 961
[25] Hoshino K, Iijima Y and Hirano K I 1980 *Trans. Japan. Inst. Met.* **21** 674
[26] Hoshino K, Iijima Y and Hirano K I 1981 *Trans. Japan. Inst. Met.* **22** 527
[27] Shimozaki T, Ito K and Onishi M 1986 *Trans. Japan. Inst. Met.* **27** 160
[28] Shimozaki T, Ito K and Onishi M 1987 *Trans. Japan. Inst. Met.* **28** 457
[29] Hagenschulte H and Heumann Th 1989 *J. Phys.: Condens. Matter* **1** 3601
[30] Hagenschulte H 1992 *PhD Thesis* Universität Münster
[31] Peterson N L and Rothman S J 1970 *Phys. Rev.* B **1** 3264
[32] Beke D L, Gödeny I, Kedves F J and Groma G 1977 *Acta Metall.* **25** 539
[33] Lundy T S and Murdock J F 1962 *J. Appl. Phys.* **33** 1671
[34] Beyeler M and Adda Y 1968 *J. Physique* **29** 345
[35] Dais S, Messer R and Seeger A 1987 *Mater. Sci. Forum* **15–18** 419
[36] Hagenschulte H and Heumann Th 1989 *Phys. Status Solidi* b **154** 71
[37] Heumann Th 1989 *Z. Metallk.* **80** 67
[38] Bocquet J L 1974 *Acta Metall.* **22** 1
[39] Arnhold V, Dayananda N A and Heumann Th 1981 *Verhandlungen DPG* **VI16** 365
[40] Snead C L, Hall T M and Goland A N 1972 *Phys. Rev. Lett.* **29** 62
[41] Takamura J, Koike M and Furukawa K 1978 *J. Nucl. Mater.* **69/70** 738
[42] Perry A J 1966 *Acta Metall.* **14** 1143
[43] Doyama M 1978 *J. Nucl. Mater.* **69/70** 350
[44] Dederichs P H 1994 to be published